Supplement of Atmos. Chem. Phys., 25, 13665–13686, 2025 https://doi.org/10.5194/acp-25-13665-2025-supplement © Author(s) 2025. CC BY 4.0 License.





## Supplement of

# Effects of different emission inventories on tropospheric ozone and methane lifetime

Catherine Acquah et al.

Correspondence to: Patrick Jöckel (patrick.joeckel@dlr.de)

The copyright of individual parts of the supplement might differ from the article licence.

#### 1 Model and set-up changes in the simulations originally performed for CCMI-1 and CCMI-2022

Figure 1 in the manuscript shows that the changed prescribed emission inventories can not explain the total difference of tropospheric CH<sub>4</sub> lifetime between the EMAC simulations originally performed for CCMI-1 and CCMI-2022 (blue and black curves in Fig. 1). There have been further model developments and setup changes apart from the changed emission inventories between the simulations performed for the two phases of CCMI-1, which we address shortly in the following. We want to stress that the simulations analysed in the manuscript, EMIS-01 and EMIS-02, use an identical version of MESSy and differ only in the prescribed boundary conditions and emissions as explained in the Method's section of the main manuscript. Thus, the changes explained in the following do not explain differences between EMIS-01 and EMIS-02, but aim at understanding differences between the simulations originally performed for CCMI-1 (blue curves in Fig. 1) and EMIS-1.

Firstly, the chemical mechanism was slightly modified, but a test simulations revealed that these modifications have no effect on the tropospheric CH<sub>4</sub> lifetime.

In addition, there was a change in the cloud microphysics parameterization. In the simulations performed for CCMI-1, the temperature, specific humidity, cloud water and cloud ice from the current model time step were used, instead of from the previous model time step, which represents the ECHAM5 default. In the simulations performed for CCMI-2022 the ECHAM5 default with the prognostic variables from the previous model time step was active. This change might affect the tropospheric CH<sub>4</sub> lifetime indirectly through changes in cloud cover affecting photolysis rates or lightning NO<sub>x</sub> production.

The same parameterization for lightning  $NO_x$  emissions (Grewe et al., 2001) with the same parameters, e.g. the scaling factor for flash-frequency, was used for the simulations for CCMI-1 and CCMI-2022 shown in Figure 1. Global lightning  $NO_x$  production averaged over the years 2000 - 2010 is 4.8 Tg(N) yr<sup>-1</sup> in the simulations performed for this study (EMIS-01, EMIS-02), which is identical to the global lightning  $NO_x$  production of simulation refD1SD performed for CCMI-2022 (Jöckel, 2023). A comparable simulation performed for CCMI-1, RC1SD-base-10a, has a slightly lower lightning  $NO_x$  production of 4.5 Tg(N) yr<sup>-1</sup> for the same time period (Jöckel et al., 2016). Assuming an  $O_3$  production of 2 DU/ (Tg(N) yr<sup>-1</sup>) (Jöckel et al., 2016, based on Dahlmann et al. (2011)), this difference in lightning  $NO_x$  emissions of 0.3 Tg(N) yr<sup>-1</sup> would lead to an increase of the  $O_3$  column of 0.6 DU, and thereby to an enhanced abundance of OH and a shorter CH<sub>4</sub> lifetime accordingly.

### 2 Supplementary figures

10

25

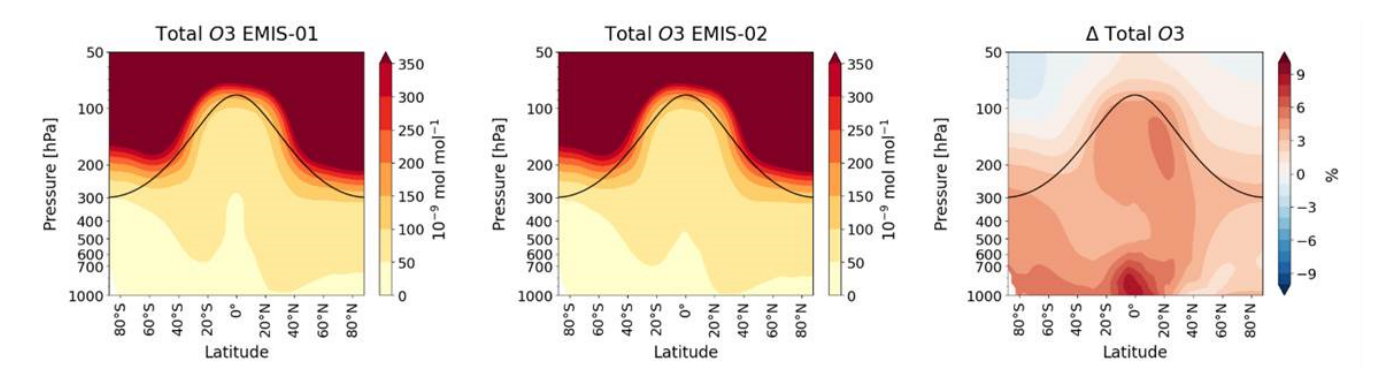
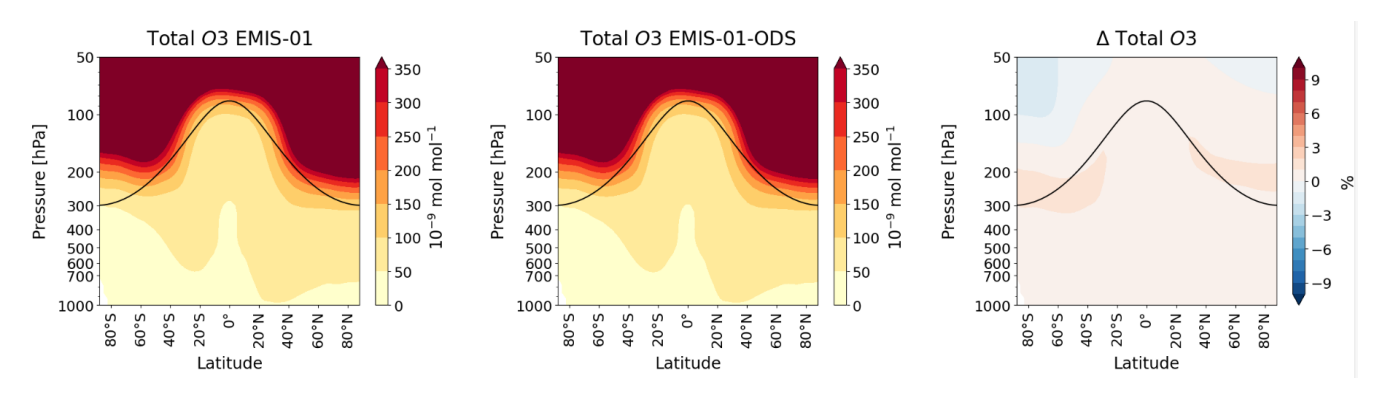


Figure S1. The zonally averaged  $O_3$  volume mixing ratios [ $10^{-9}$  mol mol<sup>-1</sup>] of simulations EMIS-01 (a) and EMIS-02 (b) and their relative difference averaged over the years 2000 - 2010 in [%].



**Figure S2.** As Fig. S1, but for the simulations EMIS-01 and EMIS-01-ODS: The zonally averaged  $O_3$  volume mixing ratios  $[10^{-9} \text{ mol mol}^{-1}]$  in the simulations EMIS-01 (a) and EMIS-01-ODS (b) and their relative difference averaged over the years 2000 - 2010 in [%].

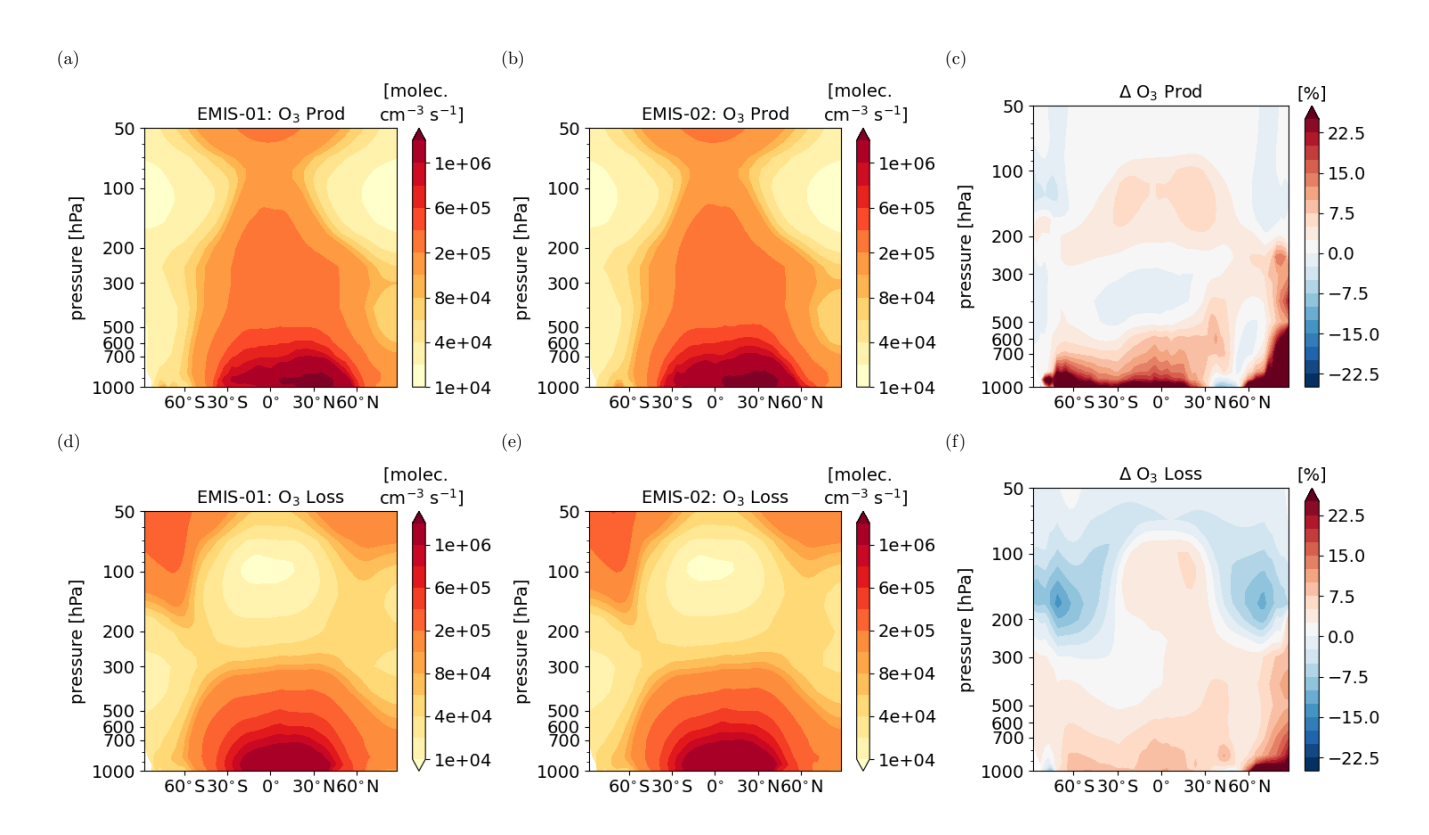


Figure S3. Multi-annual (2000 - 2010), zonally averaged effective  $O_3$  production and loss: (a)  $O_3$  production in EMIS-01, (b)  $O_3$  production in EMIS-02, (c) relative difference in  $O_3$  production in [%], (d)  $O_3$  loss in EMIS-01, (e)  $O_3$  loss in EMIS-02, and (d) relative difference in  $O_3$  loss in [%]. Note that effective  $O_3$  production and loss are shown, which means that a family that includes all fast exchanges between  $O_3$  and other species is considered (see e.g. Grewe et al., 2017). Production and loss are shown in [molecules cm<sup>-3</sup> s<sup>-1</sup>].

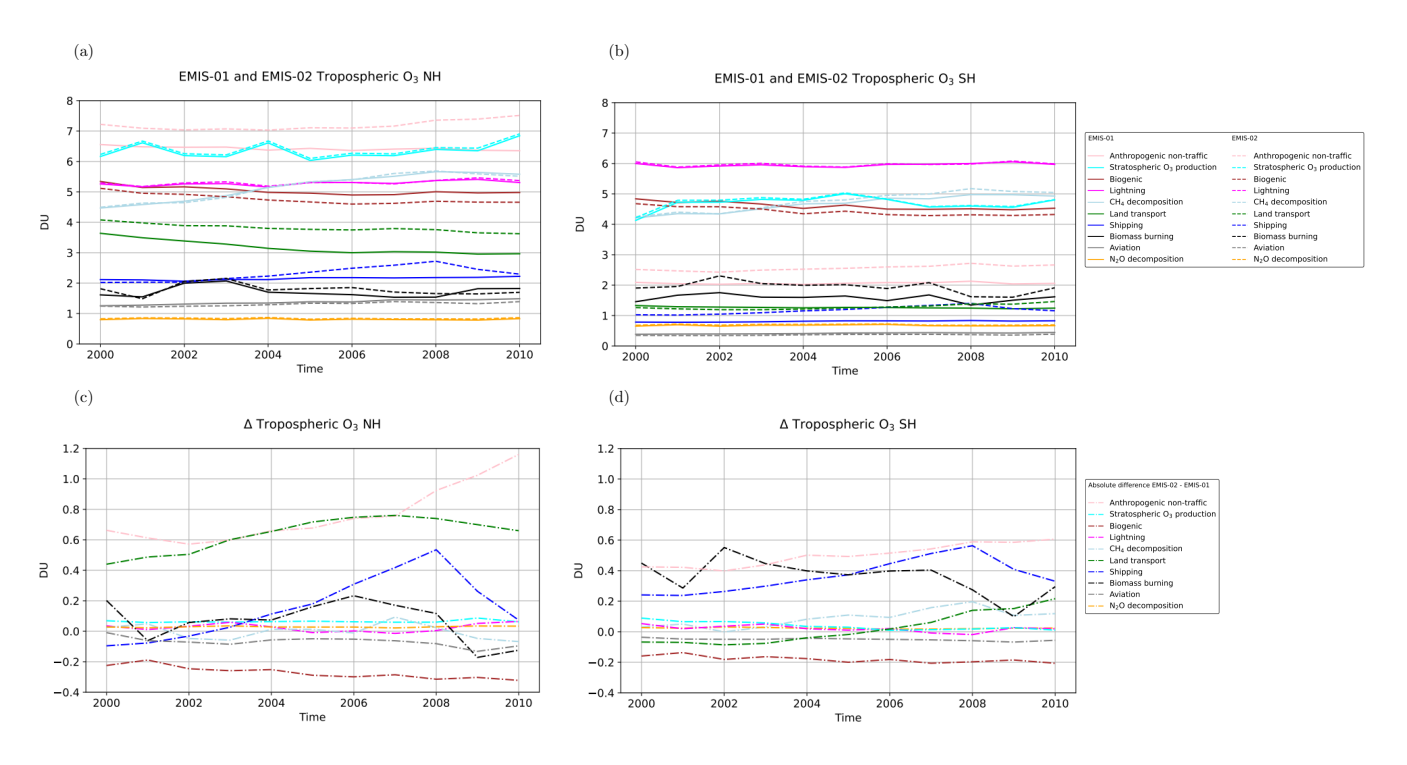


Figure S4. Time series of global mean tropospheric  $O_3$  column of the individual tagging categories in [DU] of the EMIS-01 and EMIS-02 simulation results for the period 2000 - 2010 for (a) the Northern Hemisphere and (b) the Southern Hemisphere. Panels (c) and (d) show the absolute differences in [DU] between the two simulations for the Northern Hemisphere and the Southern Hemisphere, respectively.

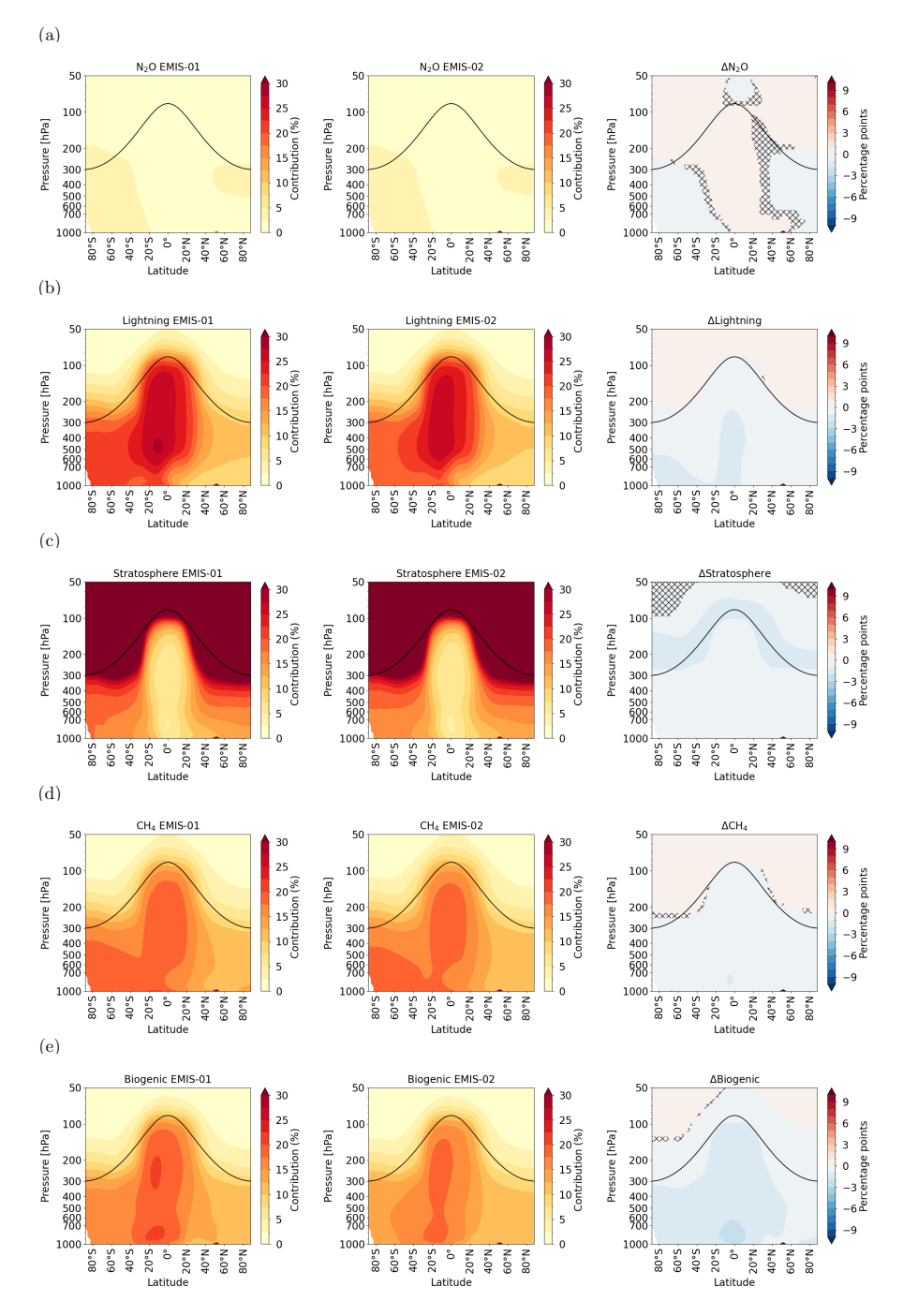
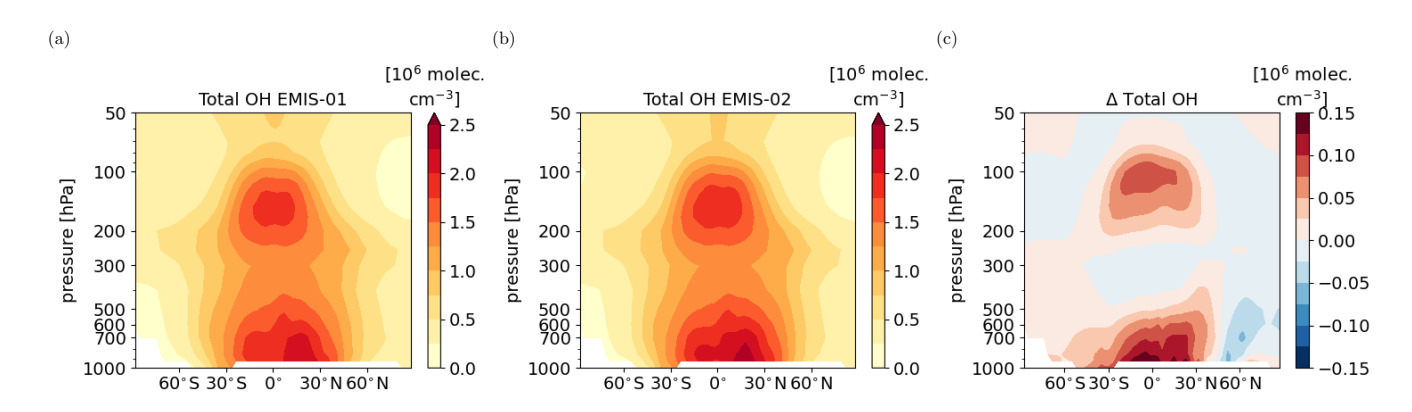


Figure S5. Relative contributions to total  $O_3$  of the tagging categories (a)  $N_2O$  decomposition, (b) lightning, (c) stratosphere (d)  $CH_4$  decomposition and (e) biogenic. The left and middle columns show the contribution of the respective category in the simulations EMIS-01 and EMIS-02, respectively. The right column shows the differences of the relative contributions to  $O_3$  between the two simulation in percentage points. Zonal means of the years 2000 - 2010 are presented. Hatches in the delta plot indicate a p-value  $\geq 0.05$  from the dependent t-test for paired samples.



**Figure S6.** Multi-annual (2000 - 2010), zonally averaged OH number concentration [ $10^6$  molecules cm<sup>-3</sup>] weighted by the reaction with CH<sub>4</sub> (see Lawrence et al., 2001) of the simulations (a) EMIS-01 and (b) EMIS-02, and (c) their absolute difference (EMIS-02 - EMIS-01).

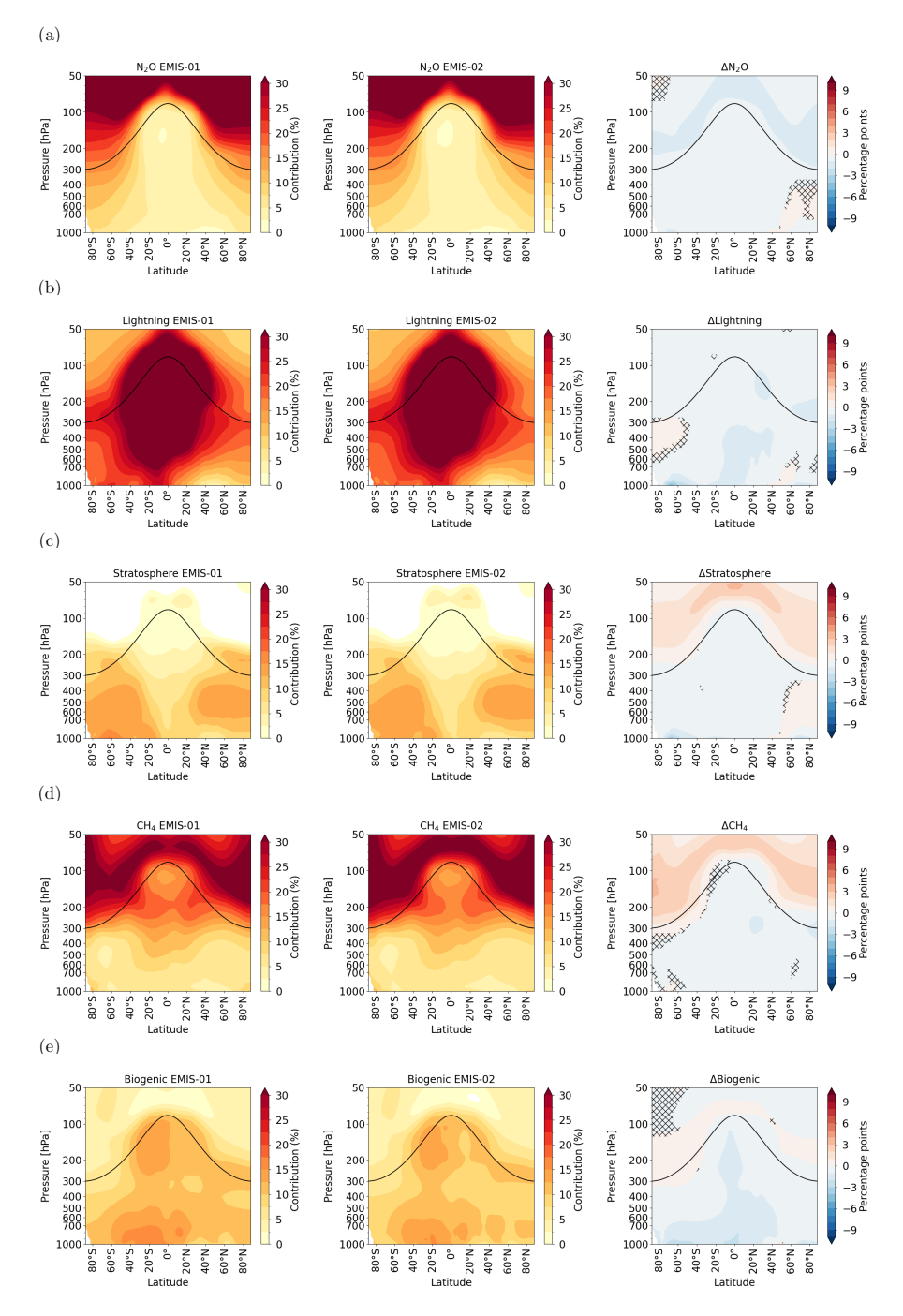


Figure S7. Relative contributions to total OH of the tagging categories (a)  $N_2O$  decomposition, (b) lightning, (c) stratosphere (d)  $CH_4$  decomposition and (e) biogenic. The left and middle columns show the contribution of the respective category in the simulations EMIS-01 and EMIS-02, respectively. The right column shows the differences of the relative contributions to OH between the two simulation in percentage points. Zonal means of the years 2000-2010 are presented. Hatches in the delta plot indicate a p-value  $\geq 0.05$  from the dependent t-test for paired samples.

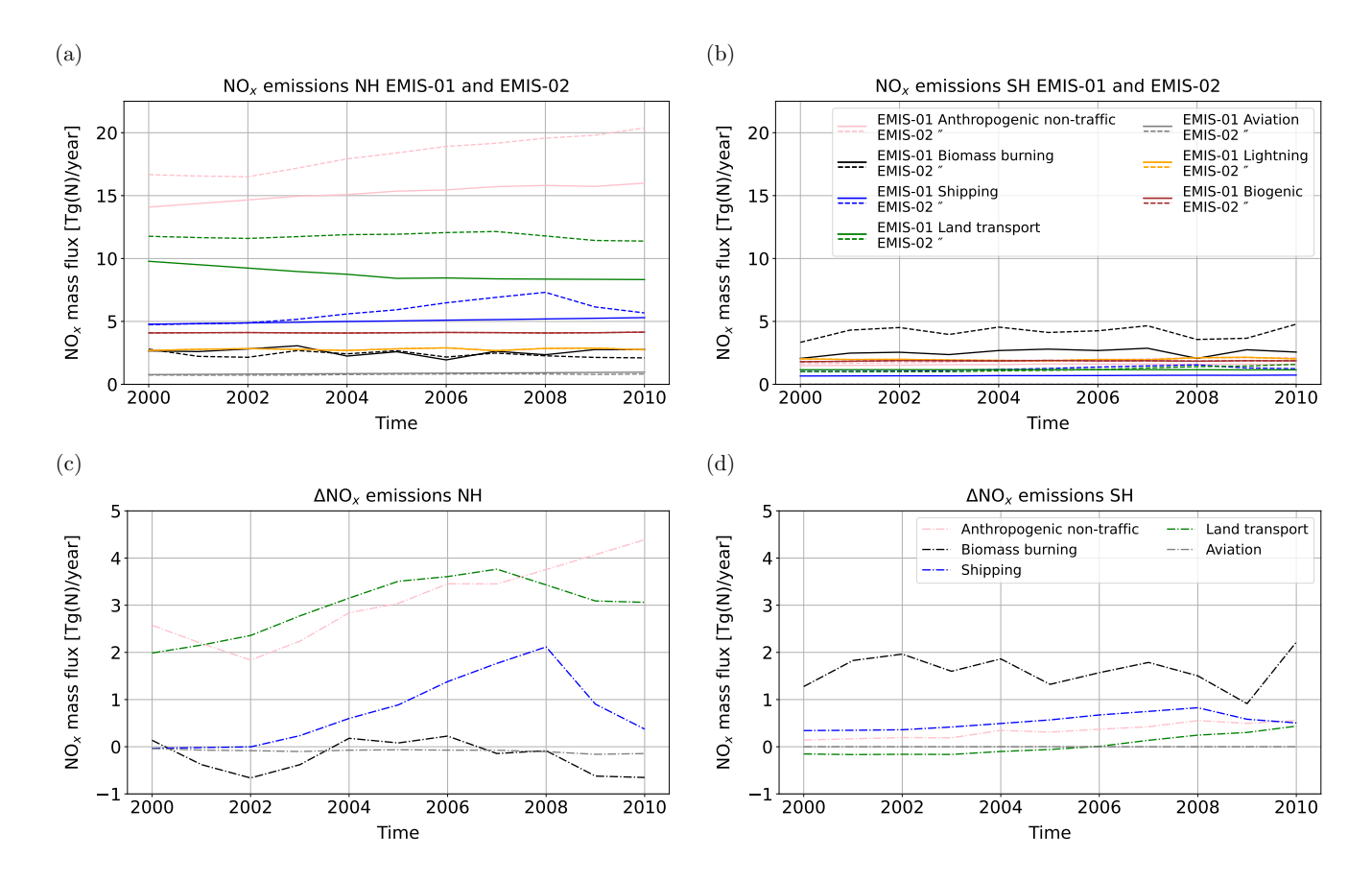
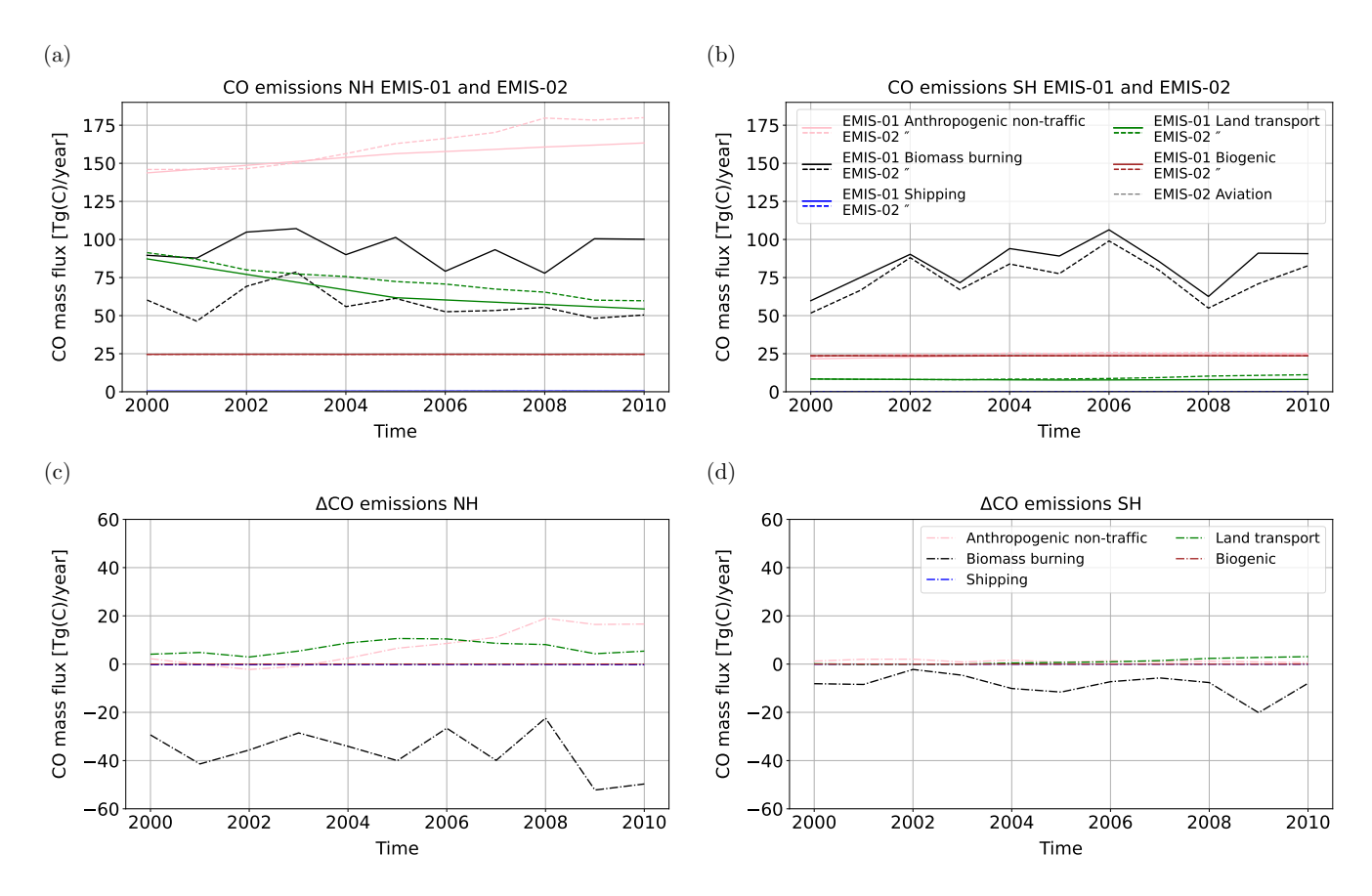
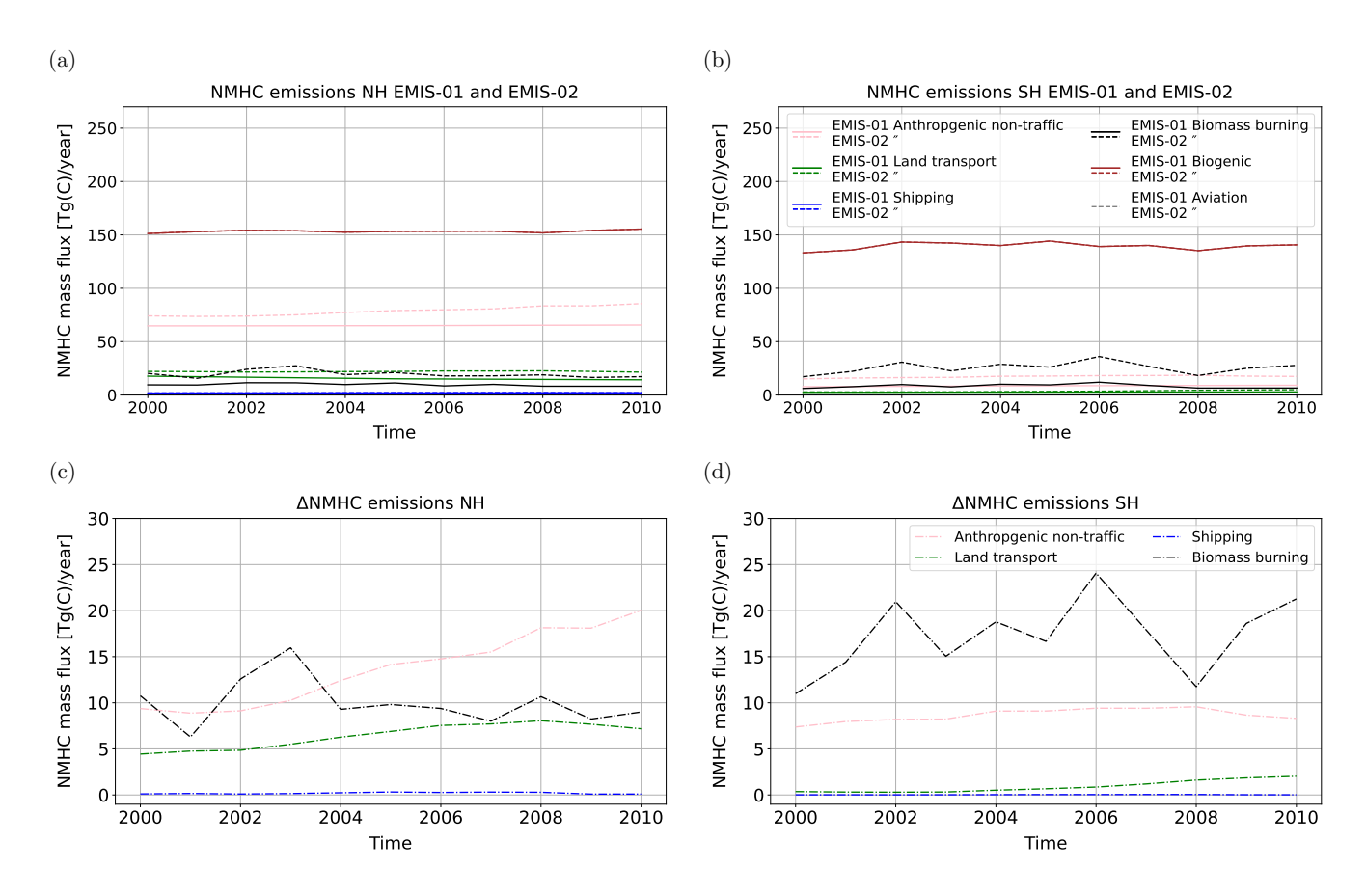


Figure S8. Time series of total  $NO_x$  emissions in  $(Tg(N) \text{ yr}^{-1})$  of the emission sectors anthropogenic non-traffic, biomass burning, shipping, land transport, aviation, lightning and biogenic prescribed or online calculated (lightning  $NO_x$  and biogenic soil  $NO_x$ ) in the simulations EMIS-01 (solid) and EMIS-02 (dashed) for the period 2000 - 2010 for (a) the Northern Hemisphere and (b) the Southern Hemisphere. Panels (c) and (d) show the absolute differences in  $(Tg(N) \text{ yr}^{-1})$  between the two simulations for the Northern Hemisphere and the Southern Hemisphere, respectively. For the sectors lightning and biogenic the emissions are identical because of the simulation set-up. Therefore, the difference is not shown for these sectors.



**Figure S9.** Time series of total CO emissions in  $(Tg(C) \text{ yr}^{-1})$  of the emission sectors anthropogenic non-traffic, biomass burning, shipping, land transport, biogenic and aviation as prescribed in the simulations EMIS-01 and EMIS-02 for the period 2000 - 2010 for (a) the Northern Hemisphere and (b) the Southern Hemisphere. Panels (c) and (d) show the absolute differences in  $(Tg(C) \text{ yr}^{-1})$  between the two simulations for the Northern Hemisphere and the Southern Hemisphere, respectively. CO emissions of the aviation sector were only considered in the emission inventory used for EMIS-02 (on average global emissions of  $0.22 \text{ Tg}(C) \text{ yr}^{-1}$  for the years 2000 - 2010). Therefore, no difference is plotted for this sector. For the sector biogenic the emissions are identical in both simulations, and, therefore, no difference is shown either.



**Figure S10.** Time series of total NMHC emissions in  $(Tg(C) \text{ yr}^{-1})$  of the emission sectors anthropogenic non-traffic, land transport, shipping, biomass burning, biogenic and aviation as prescribed in the simulations EMIS-01 and EMIS-02 for the period 2000 - 2010 for (a) the Northern Hemisphere and (b) the Southern Hemisphere. Panels (c) and (d) show the absolute differences in  $(Tg(C) \text{ yr}^{-1})$  between the two simulations for the Northern Hemisphere and the Southern Hemisphere, respectively. NMHC emissions of the aviation sector were only considered in the emission inventory used for EMIS-02 (on average global emissions of  $0.07 \text{ Tg}(C) \text{ yr}^{-1}$  for the years 2000 - 2010). Therefore, no difference is plotted for this sector. For the sector biogenic the emissions are identical in both simulations, and, therefore, no difference is shown either.

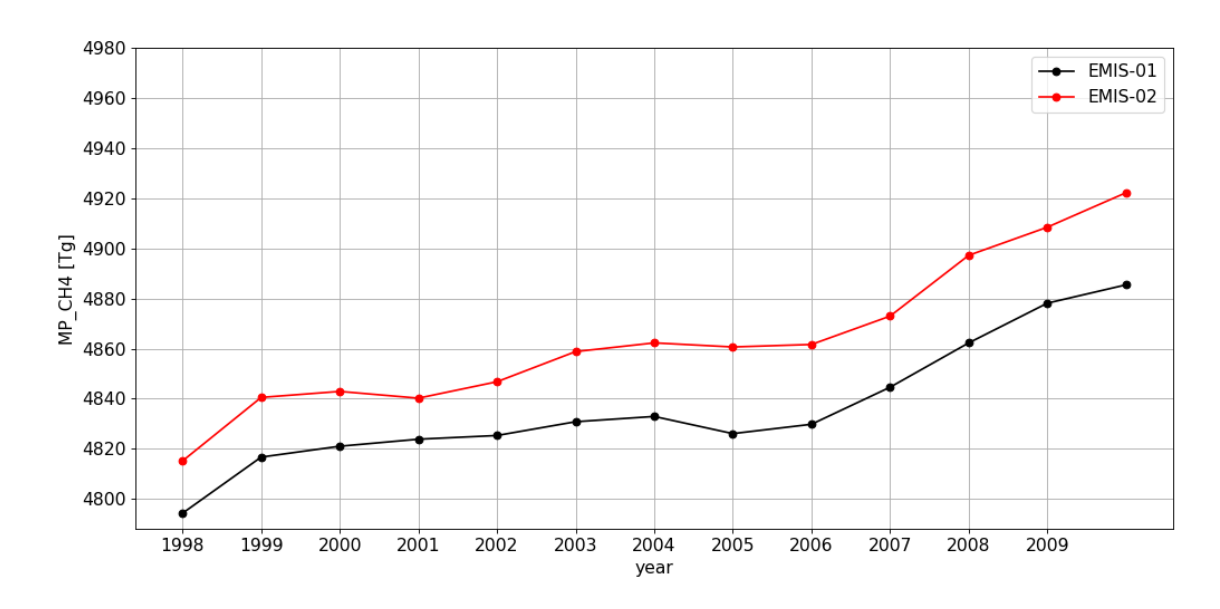


Figure S11. Total atmospheric mass of CH<sub>4</sub> in Tg.

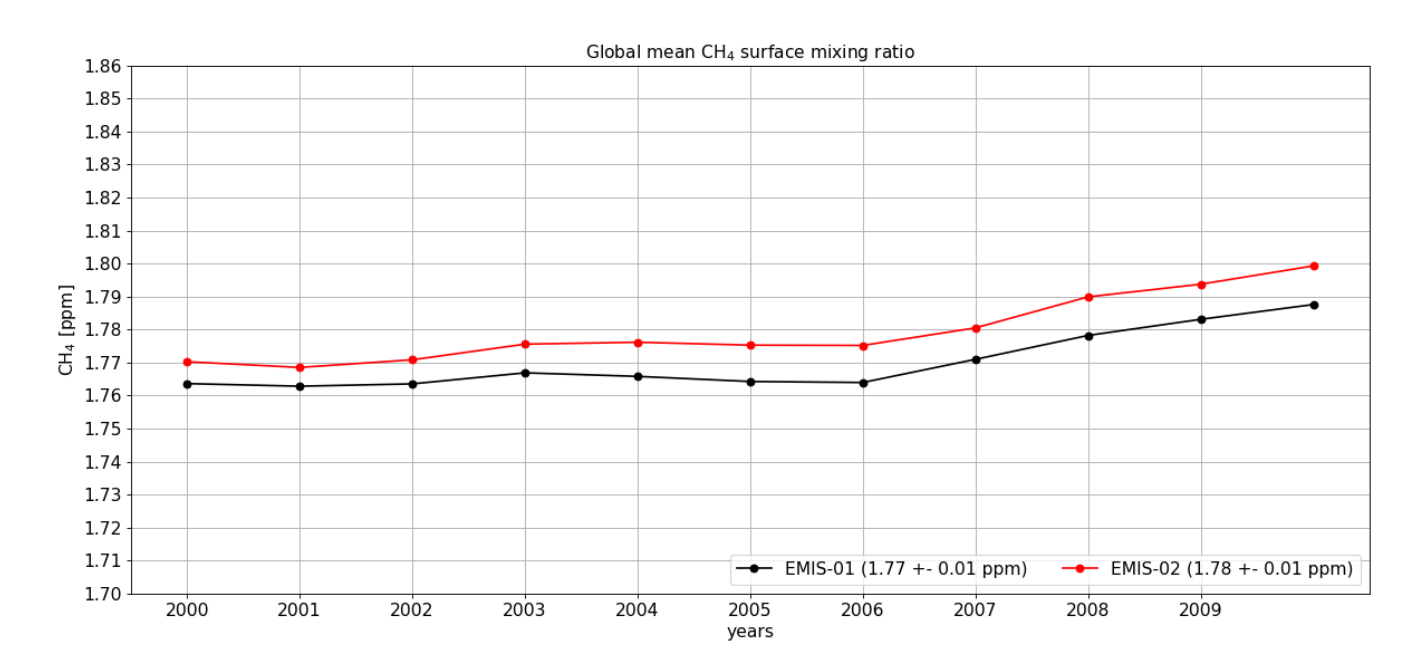


Figure S12. Global mean surface CH<sub>4</sub> mixing ratio in ppm.

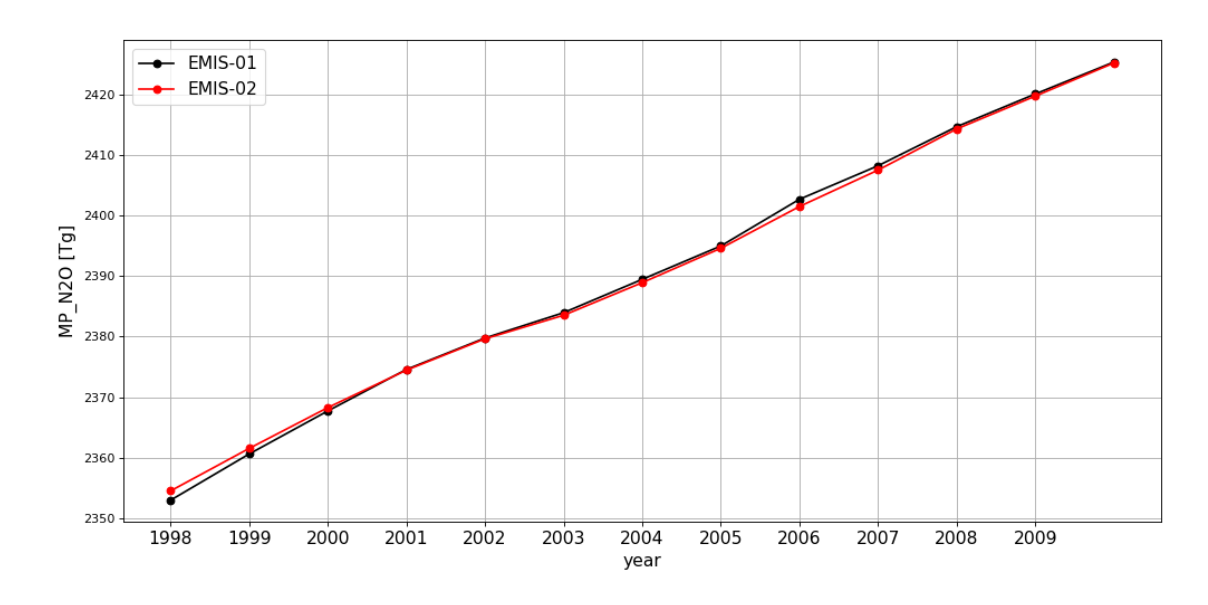
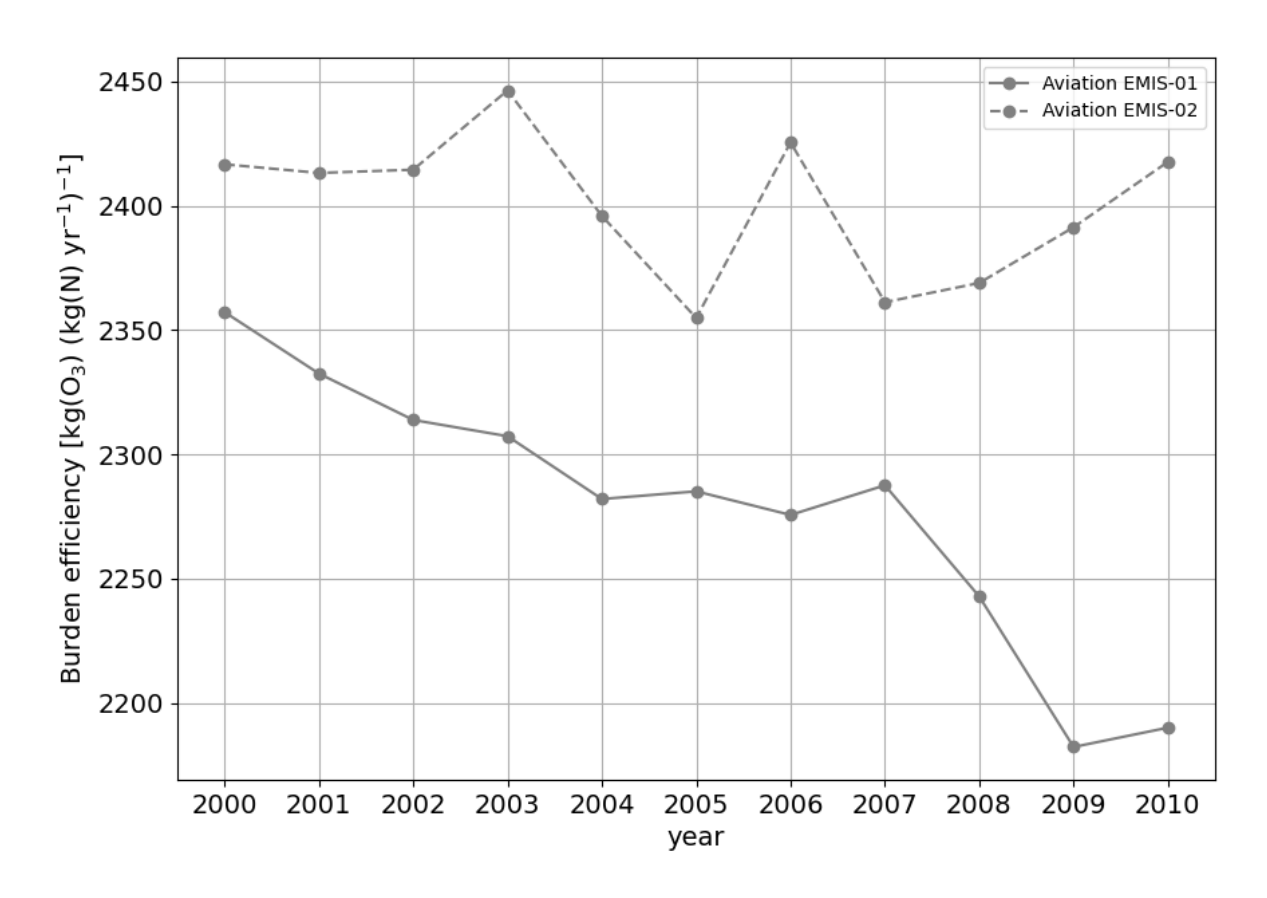


Figure S13. Total atmospheric mass of  $N_2O$  in Tg.



**Figure S14.** Global burden efficiency  $\chi^{air}$  of the aviation category (in kg(O<sub>3</sub>) (kg(N) yr<sup>-1</sup>)<sup>-1</sup>).

#### References

40

- Dahlmann, K., Grewe, V., Ponater, M., and Matthes, S.: Quantifying the contributions of individual NOx sources to the trend in ozone radiative forcing, Atmospheric Environment, 45, 2860–2868, https://doi.org/10.1016/j.atmosenv.2011.02.071, 2011.
- Grewe, V., Brunner, D., Dameris, M., Grenfell, J. L., Hein, R., Shindell, D., and Staehelin, J.: Origin and variability of upper tropospheric nitrogen oxides and ozone at northern mid-latitudes, Atmospheric Environment, 35, 3421–3433, https://doi.org/10.1016/s1352-2310(01)00134-0, 2001.
  - Grewe, V., Tsati, E., Mertens, M., Fromming, C., and Jockel, P.: Contribution of emissions to concentrations: the TAGGING 1.0 submodel based on the Modular Earth Submodel System (MESSy 2.52), Geoscientific Model Development, 10, 2615–2633, https://doi.org/10.5194/gmd-10-2615-2017, 2017.
- Jöckel, P.: CCMI-2022: refD1 data produced by the EMAC-CCMI2 model at MESSy-Consortium, https://catalogue.ceda.ac.uk/uuid/9b15ae551fda4035a7940a3adbe31691/, 2023.
  - Jöckel, P., Tost, H., Pozzer, A., Kunze, M., Kirner, O., Brenninkmeijer, C. A. M., Brinkop, S., Cai, D. S., Dyroff, C., Eckstein, J., Frank, F., Garny, H., Gottschaldt, K. D., Graf, P., Grewe, V., Kerkweg, A., Kern, B., Matthes, S., Mertens, M., Meul, S., Neumaier, M., Nutzel, M., Oberländer-Hayn, S., Ruhnke, R., Runde, T., Sander, R., Scharffe, D., and Zahn, A.: Earth System Chemistry integrated Modelling (ESCiMo) with the Modular Earth Submodel System (MESSy) version 2.51, Geoscientific Model Development, 9, 1153–1200, https://doi.org/10.5194/gmd-9-1153-2016, 2016.
  - Lawrence, M. G., Jöckel, and von Kuhlmann, R.: What does the global mean OH concentration tell us?, Atmos. Chem. Phys., 1, 37–49, https://doi.org/10.5194/acp-1-37-2001, 2001.